JEM

Supplemental material

Basheer et al., **https://doi.org/10.1084/jem.20181276**

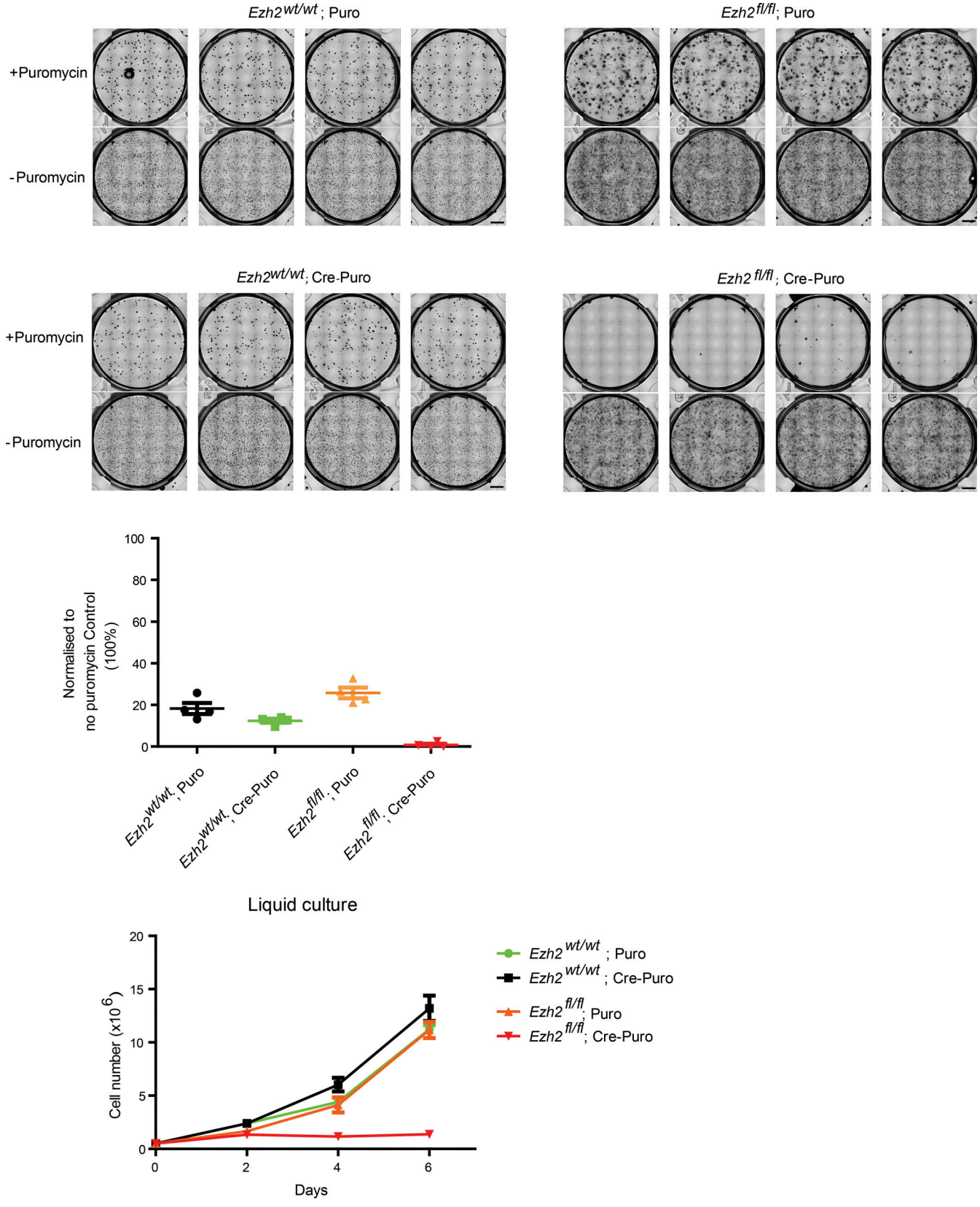

Figure S1. **Transduction efficiency and Cre-recombinase toxicity in *Ezh2*$^{wt/wt}$ and *Ezh2*$^{fl/fl}$ MLL-AF9–transformed cell lines**. Related to Fig. 1 (b–d). Top: Colony-forming assays of *Ezh2*$^{wt/wt}$ (left) and *Ezh2*$^{fl/fl}$ (right) murine cells transformed with MLL-AF9, transduced with p-babe-Cre-puro or p-babe-puro (empty vector), and plated with or without puromycin (1 µg/ml). Bars, 4 mm. Middle: Number of colonies normalized to "no puromycin" control. Bottom: Growth curves of *Ezh2*$^{wt/wt}$ and *Ezh2*$^{fl/fl}$ murine cells transformed with MLL-AF9, transduced with p-babe-Cre-puro or p-babe-puro (empty vector), and maintained in liquid culture in the presence of puromycin (1 µg/ml). All error bars are ± SEM.

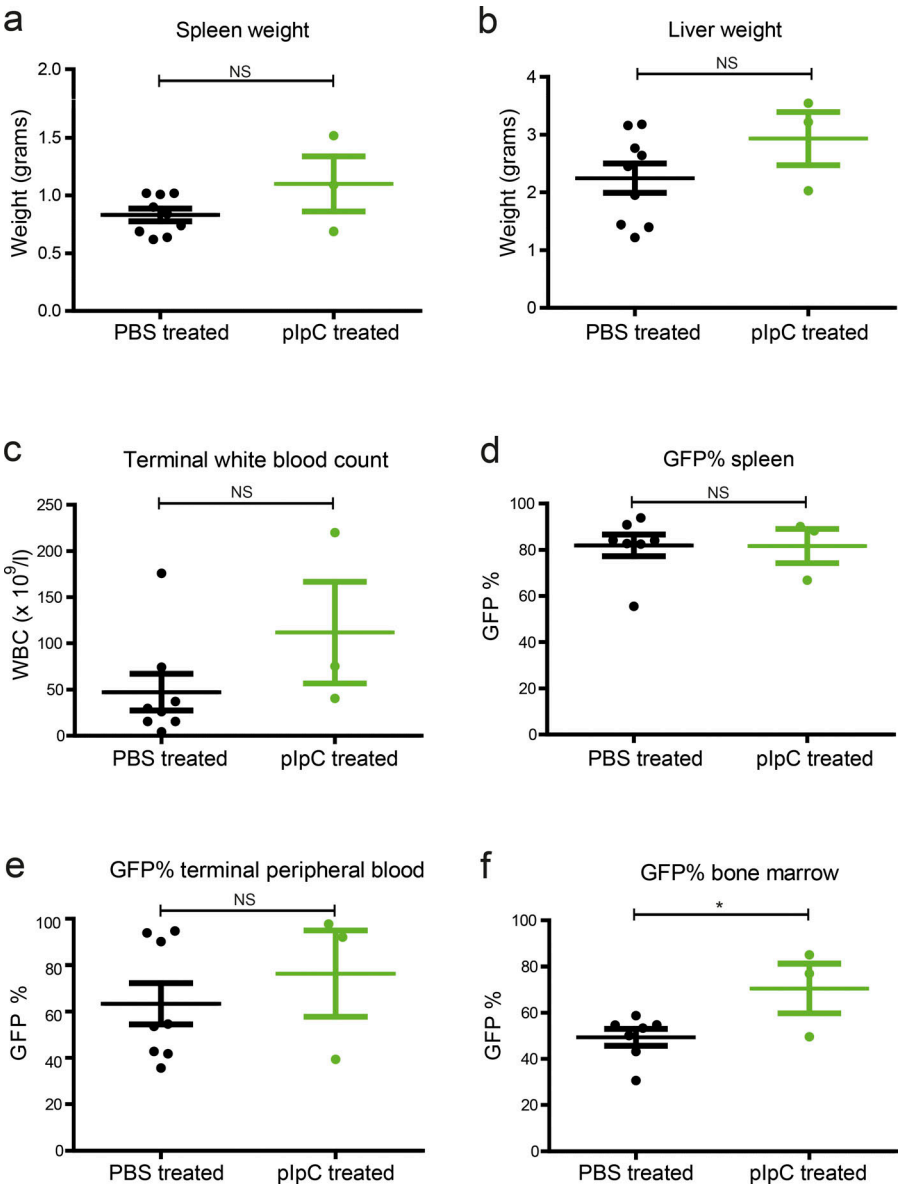

Figure S2. **AML1-ETO9a secondary murine leukemia characteristics at necropsy.** Related to Fig. 1 f. **(a and b)** Spleen and liver weights for PBS (n = 9)– and pIpC (n = 3)–treated *Ezh2*$^{-/-}$;*Mx1-Cre*$^{+}$ AML1-ETO9a secondary GFP^{+} leukemias. **(c)** Total terminal white blood cell counts for PBS (n = 8)– and pIpC (n = 3)–treated GFP^{+} leukemias. **(d–f)** GFP positivity in spleen, BM (P = 0.0393), and terminal peripheral blood of PBS (n = 8)– vs. pIpC (n = 3)–treated GFP^{+} leukemias, reflecting tumor burden. All tests were two-tailed t tests. *, P < 0.05. All error bars are ± SEM.

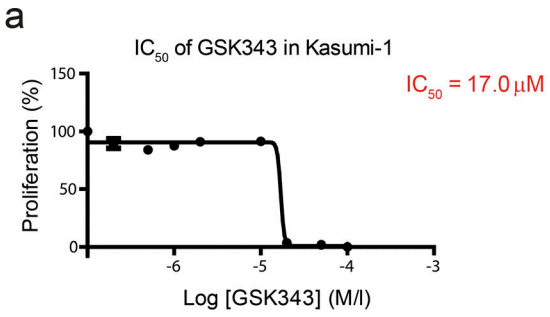

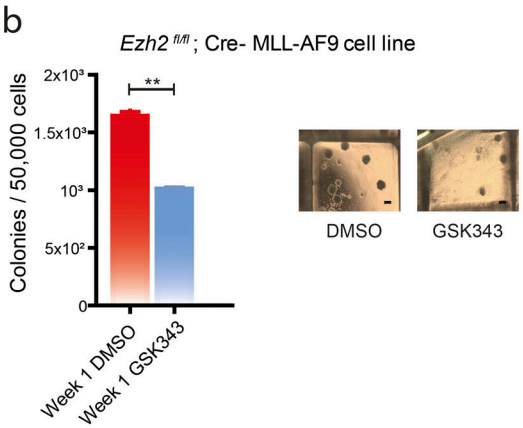

c

Patient	Sex	Age	Karyotype/Cytogenetic abnormality
1	M	83	N/A
2	F	45	Trisomy 15
3	F	59	N/A
4	M	74	46, XY
5	M	21	Monosomy 1p and trisomy 8q
6	M	65	46, XY
7	F	70	Complex
8	M	66	Trisomy 8 in 2 of 22 cells (47, XY, +8[2]/46, XY[20])
9	F	46	46, XX
10	F	65	46, XX
11	M	38	46, XY
12	F	56	Complex
13	M	63	APML - PML/RARA detected
14	M	20	MLL -AF9 translocated
15	M	22	46, XY

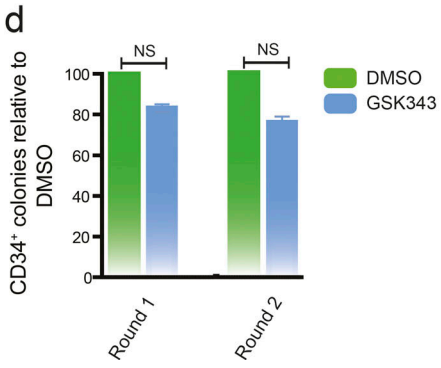

Figure S3. **GSK343 activity against human AML cell lines, immortalized murine cell lines, and primary human CD34⁺/AML samples.** Related to Fig. 2. **(a)** Cell proliferation assay for Kasumi-1 cell line at 72 h across GSK343 concentrations 100 nM to 100 µM demonstrating IC_{50} value of 17 µM (logarithmic scale, x axis, *n* = 3 technical replicates). **(b)** Immortalized *Ezh2*$^{+/+}$ MLL-AF9 lines exhibit reduced colony formation at 1 wk with GSK343 (10 µM) treatment compared with DMSO control (*n* = 3, P < 0.0024, two-tailed *t* test). Photomicrograph inserts demonstrate that GSK343 treatment results in smaller colony size and colony number (representative first-round colonies per genotype/treatment are shown; bars, 500 µm). **(c)** Demographics and karyotypic/cytogenetic abnormalities for fifteen human AML primary samples displaying sensitivity to GSK343 in colony-forming cell assays (related to Fig. 2 g). F, female; M, male; N/A, not applicable. **(d)** GSK343 does not exhibit significant toxicity to normal human CD34⁺ cells. DMSO was used as control. Colonies counted 7–10 d after seeding 50,000 cells per methylcellulose plate. Normalized data are shown; P = NS by two-sided *t* test. **, P < 0.001. All error bars are ± SEM.

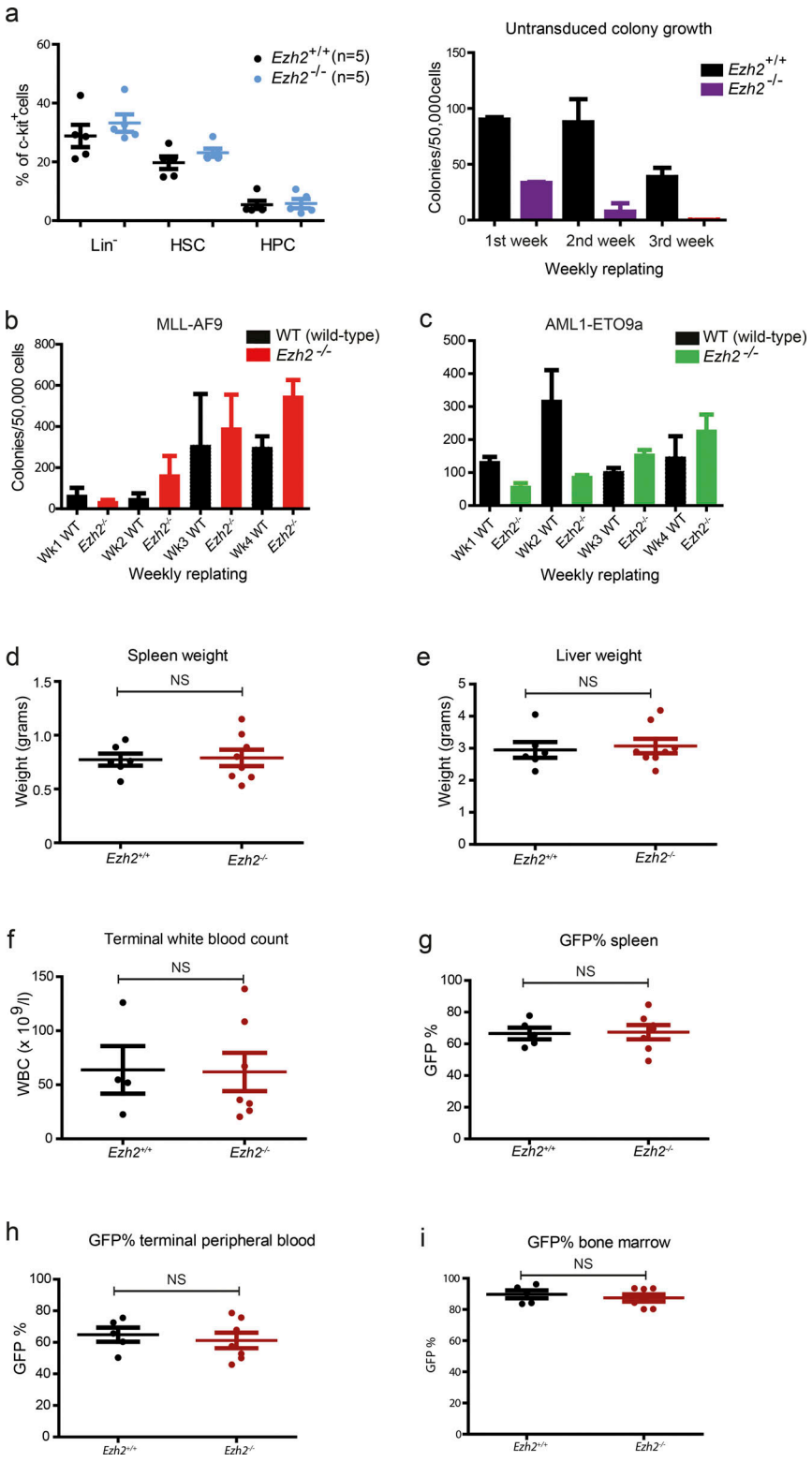

Figure S4. ***Ezh2* during AML induction.** Related to Fig. 3. **(a)** Left: Immunophenotyping panels of c-kit⁺ populations derived from BM of *Ezh2*$^{+/+}$ (n = 5) and *Ezh2*$^{-/-}$ (n = 5) mice showing Lin⁻, HSC, and hematopoietic progenitor cell proportions between each genotype. Right: Colony-forming cell assay demonstrating colony growth through weekly replatings of untransduced *Ezh2*$^{+/+}$ (n = 5) and *Ezh2*$^{-/-}$ (n = 4) BM cells. **(b)** Serial replating assay of WT (WT or *Ezh2*$^{fl/fl;}$ *Mx1-Cre*⁻) MLL-AF9 transduced against *Ezh2*$^{-/-}$ (*Ezh2*$^{fl/fl}$; *Mx1-Cre*⁺ and pIpC treated) MLL-AF9–transduced c-kit⁺ BM cells. **(c)** Serial replating assay of WT (WT or *Ezh2*$^{fl/fl}$; *Mx1-Cre*⁻) AML1-ETO9a–transduced against *Ezh2*$^{-/-}$ (*Ezh2*$^{fl/fl}$; *Mx1-Cre*⁺ heterozygous and pIpC-treated) AML-ETO9a–transduced c-kit+ BM cells. **(d and e)** Spleen and liver weights for *Ezh2*$^{+/+}$ (n = 7) and *Ezh2*$^{-/-}$ (n = 8) MLL-AF9 leukemias. **(f)** Total terminal white blood cell count for *Ezh2*$^{+/+}$ (n = 4) and *Ezh2*$^{-/-}$ (n = 7) MLL-AF9 leukemias. **(g–i)** GFP positivity in spleen, BM, and terminal peripheral bleeds (after red cell lysis step) of *Ezh2*$^{+/+}$ (n = 5) vs. *Ezh2*$^{-/-}$ (n = 7) treated leukemias, reflecting tumor burden. All error bars are ± SEM.

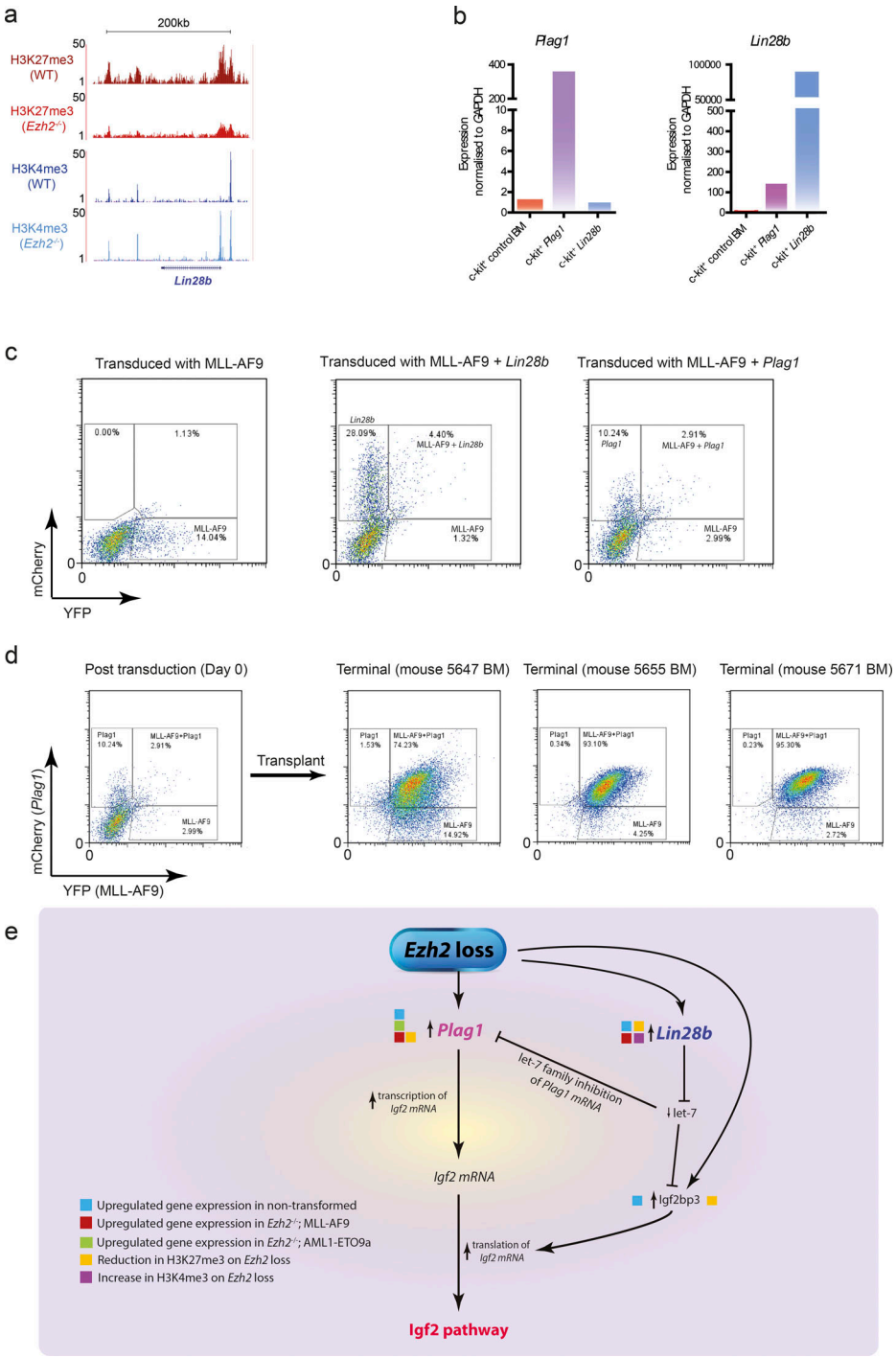

Figure S5. **Functional validation of *Plag1/Lin28b* as downstream mechanistic effectors of *Ezh2* loss.** Related to Fig. 5 (g and h). **(a)** ChIP-seq analysis of H3K27me3 and H3K4me3 chromatin marks reveals resolution of conflicting histone marks H3K27me3 and H3K4me3 at the bivalent promoter region in favor of gene activation, with decreased H3K27me3 and increased H3K4me3, for the oncogene *Lin28b* in WT murine Lin⁻ BM HSPCs following *Ezh2* loss, explaining its increased expression. **(b)** qRT-PCR in c-kit selected WT HSPCs demonstrating expression levels of *Plag1* and *Lin28b* following transduction with MSCV-*Plag1*-IRES-mCherry (left) and MSCV-*Lin28b*-IRES-mCherry construct (right). As expected, *Plag1* and *Lin28b* are overexpressed in the left and right panels, respectively; however, as shown in the right panel, *Plag1* is also up-regulated in MSCV-*Lin28b*-IRES-mCherry–transduced cells. All transcripts are normalized to *Gapdh*. **(c)** Transduction efficiencies of MSCV-MLL-AF9-IRES-YFP single vs. dual MLL-AF9/*Lin28b* and dual MLL-AF9/*Plag1*–transduced c-kit⁺ BM HSPCs. **(d)** Expansion of dual-transduced (MLL-AF9/*Plag1*) cells isolated from BM at necropsy of leukemic mice (three representative examples shown, on right) compared with single MLL-AF9–expressing leukemia cells compared with cells initially transplanted (left panel). **(e)** Proposed molecular model of *Ezh2* loss and downstream effects. *Ezh2* loss leads to direct up-regulation of *Plag1* and *Lin28b* through loss of H3K27me3 and an increase in H3K4me3 (for *Lin28b*) at their bivalent promoters. *Lin28b* overexpression negatively regulates maturation of the let-7 miRNA family, releasing let-7 inhibition on *Igf2bp3* and *Plag1*. *Plag1* and *Igf2bp3* cooperate to potentially drive the Igf2 axis through increased transcription and translation of *Igf2* mRNA, respectively, and contribute to accelerated and poor-prognosis AML.

Tables S1–S8 are provided online as separate Excel files. Table S1 lists the causes of death for animals on the AML1-ETO9a maintenance experiments. Table S2 lists the differentially expressed genes in *Ezh2*$^{+/+}$ MLL-AF9 mouse tumors treated with GSK343 (vs. DMSO). Table S3 lists the differentially expressed genes in *Ezh2*$^{+/+}$ vs. *Ezh2*$^{-/-}$ Lin$^-$ BM cells (HSPCs). Table S4 lists the differentially expressed genes in *Ezh2*$^{+/+}$ vs. *Ezh2*$^{-/-}$ AML1-ETO9a BM cells. Table S5 lists the differentially expressed genes in *Ezh2*$^{+/+}$ vs. *Ezh2*$^{-/-}$ MLL-AF9 BM cells. Table S6 lists the differentially bound peaks for H3K27me3 between *Ezh2*$^{+/+}$ vs. *Ezh2*$^{-/-}$ BM HSPCs. Table S7 lists the differentially bound peaks for H3K4me3 between *Ezh2*$^{+/+}$ vs. *Ezh2*$^{-/-}$ BM HSPCs. Table S8 lists the differentially bound peaks for H3K27Ac between *Ezh2*$^{+/+}$ vs. *Ezh2*$^{-/-}$ BM HSPCs.